P-wave complexity in normal subjects and computer models

Mark Potse, Theo Lankveld, Stef Zeemering, Pieter Dagnelie, Coen Stehouwer, Ronald Henry, André Linnenbank, Nico Kuijpers, Ulrich Schotten

Available online at www.sciencedirect.com

ScienceDirect

Journal of Electrocardiology 49 (2016) 545 – 553

JOURNAL OF Electrocardiology

www.jecgonline.com

P-wave complexity in normal subjects and computer models

Mark Potse, PhD,[a,*,1] Theo A.R. Lankveld, MD,[b] Stef Zeemering, PhD,[c] Pieter C. Dagnelie, PhD,[d,e,f] Coen D.A. Stehouwer, MD, PhD,[e,g] Ronald M. Henry, MD, PhD,[e,g] André C. Linnenbank, PhD,[h] Nico H.L. Kuijpers, PhD,[a] Ulrich Schotten, MD, PhD[c]

[a] *Department of Biomedical Engineering, Cardiovascular Research Institute Maastricht, Maastricht University, Universiteitssingel 50, 6229 ER Maastricht, The Netherlands*

[b] *Department of Cardiology, Cardiovascular Research Institute Maastricht, Maastricht University, Universiteitssingel 50, 6229 ER Maastricht, The Netherlands*

[c] *Department of Physiology, Cardiovascular Research Institute Maastricht, Maastricht University, Universiteitssingel 50, 6229 ER Maastricht, The Netherlands*

[d] *Department of Epidemiology, Maastricht University*

[e] *CARIM School for Cardiovascular Diseases, Maastricht University*

[f] *CAPHRI School for Public Health and Primary Care, Maastricht University*

[g] *Department of Internal Medicine, Maastricht University Medical Centre*

[h] *Heart Center, Academic Medical Center, University of Amsterdam, Amsterdam, The Netherlands*

Abstract

Background: P waves reported in electrocardiology literature uniformly appear smooth. Computer simulation and signal analysis studies have shown much more complex shapes.

Objective: We systematically investigated P-wave complexity in normal volunteers using high-fidelity electrocardiographic techniques without filtering.

Methods: We recorded 5-min multichannel ECGs in 16 healthy volunteers. Noise and interference were reduced by averaging over 300 beats per recording. In addition, normal P waves were simulated with a realistic model of the human atria.

Results: Measured P waves had an average of 4.1 peaks (range 1–10) that were reproducible between recordings. Simulated P waves demonstrated similar complexity, which was related to structural discontinuities in the computer model of the atria.

Conclusion: The true shape of the P wave is very irregular and is best seen in ECGs averaged over many beats.

Keywords: Electrocardiogram; P wave; Interatrial block; Filtering; Recording techniques; Computer models

Introduction

On the routine electrocardiogram (ECG), P waves usually have a smooth appearance [1]. A notched or more complex P-wave shape is thought to be an abnormal finding. A previous study even found notched P waves to be a predictor of cardiovascular events [2]. Furthermore, changes in P-wave morphology are associated with interatrial block [3], a known predictor for supraventricular tachyarrhythmias [4,5] and electromechanical dysfunction of the left atrium [6].

However, recent computer modeling studies have predicted highly complex P-wave shapes in normal atria [7,8]. Details of these P waves were linked to normal structural features of the atria. More complex shapes have also been observed in advanced signal-analysis studies [9–11].

Prompted by these conflicting reports we tested if complex P-wave shapes are present in healthy subjects. We studied normal young and aged volunteers using 5-min multichannel high-resolution surface ECGs. We avoided low-pass filters, because these may remove high-frequency signal content along with the noise, while being unable to remove interference with lower frequencies. Instead, noise suppression was achieved by a careful P-wave alignment and averaging procedure resulting in

* Corresponding author at: Inria Bordeaux Sud-Ouest, 200 Avenue de la vieille tour, 33405 Talence Cedex, France.

E-mail address: mark@potse.nl

[1] Present address: LIRYC – Institute for Cardiac Rhythmology and Modeling; Carmen Team, Inria Bordeaux Sud-Ouest, Bordeaux, France; and Center for Computational Medicine in Cardiology, Institute of Computational Science, Università della Svizzera italiana, Lugano, Switzerland.

http://dx.doi.org/10.1016/j.jelectrocard.2016.05.005

an ECG with microvolt-level fidelity. We compared the measured P waves with those predicted by a computer simulation study involving a structurally realistic anatomical model of the human atria.

Methods

Measurements

Multichannel ECGs from 184 thoracic electrodes [12] and 3 limb electrodes were recorded in two groups:

- A "young" group consisting of seven healthy volunteers (Y1–Y7), all male, aged 26–43 years (average 30).
- A "senior" group consisting of seven male and two female subjects (S1–S9) aged 61–72 years (average 67) with normal cardiac anatomy and function who entered the Maastricht Study, a population-based cohort study on the development of chronic diseases [13]. The Maastricht Study has been approved by the ethical committee of Maastricht University Medical Center. All participants gave written informed consent. Subject S9 was diabetic.

Recordings were made using a 256-channel Biosemi ActiveTwo amplifier (Biosemi, Amsterdam, The Netherlands) with 0.8 μV root-mean-square noise level. Signals were low-pass filtered (3 dB point 419 Hz) and digitized at a frequency of 2048 Hz with 0.03 μV resolution.

Signals from electrodes with poor contact and intervals of recording with excessive artifacts were manually removed. QRS peaks were detected using an energy signal, similar to that used by Pan and Tompkins [14], based on the temporal derivatives of the 184 thoracic leads. A time instant for baseline correction was chosen manually shortly before the P-wave onset, and a piecewise linear baseline correction was applied to the entire recording. The detected QRS peaks were used for an initial alignment of the beats. A P-wave template was chosen manually, and the remaining beats were shifted to maximize correlation of the P wave with the template. This procedure was performed on the sum squared voltages of the thoracic leads to reduce the effect of noise on the alignment. An average P wave was then computed and used as a template in a second alignment step. P waves that correlated less than a preset threshold of 0.9 with the template were excluded from this averaging. The final averaged PQRST complex was used for analysis. To avoid influence of mains interference on the alignment process, a notch filter at 50 Hz and multiples thereof was applied to the raw data. This filter affected only the signals used for beat detection and alignment; the final averaging took place on unfiltered data.

To quantify the complexity of the signals we automatically counted the peaks (positive and negative) in each P wave. The algorithm first determined all local extrema, defined as samples that had either a higher value than the preceding and following sample, or a lower value than both. Then it identified all pairs of successive extrema with voltage values that were closer than a given threshold, and repeatedly removed the pair with the smallest absolute difference until no subthreshold differences remained.

We report the number of peaks determined with each of two methods to set the threshold for the definition of a peak: it was either fixed at 10 μV or determined by an estimate of the variability in the signal. This estimate was obtained by performing the alignment and averaging procedure described above on five randomly determined subsets of beats. The maximum difference between the five resulting averages and the global average signal was then used as the variability measure. Since the variability in the global average should be smaller than the variability in the group averages, this yields an overestimation of the variability, and therefore an underestimation of the number of peaks. The advantage of this conservative estimate is that it identifies with certainty a lower bound on the number of peaks that are invariable, i.e. should be reproducible between repeated measurements in the same subject.

To find inter-subject similarities in the pattern of notching we considered the timing of the notches, in all 12 leads combined. Initially, peak and nadir times for all subjects combined were counted in 10-millisecond bins. Adjacent bins with similar counts were then combined and bin edges were adapted to identify intervals of high and low notch density. The number of notches in each of the new bins was then determined for each subject individually, and a mean value and standard deviation for each bin were computed.

P-wave duration was difficult to measure because there was no instant in the P-Q interval where all signals were zero. Therefore we measured it manually using digital calipers in a signal prepared from the sum of the absolute values of all leads, after averaging. P-wave onset was defined as the start of the first clear upstroke of the signal, and P-wave end as a local minimum after which rapid signal changes ceased.

From the 184 thoracic electrodes we selected those that were closest to the standard precordial positions [12]. Together with the limb leads these were used to create a standard 12-lead ECG.

Simulations

An anatomical model of the human atria was built using Blender (The Blender Foundation, Amsterdam, The Netherlands) as a 3-D editing tool. The global shape was guided by MRI data from a subject with normal atrial anatomy. Details were filled in based on literature [15–17]. As illustrated in Fig. 1, this model consisted of surfaces representing the endocardial surface of the atria, pulmonary and caval veins, and coronary sinus; an "envelope" for the atrial myocardium; and several bundles representing thicker parts of the atrial myocardium such as the crista terminalis, the pectinate muscles, and the superior and posterior wall of the left atrium. Also included were a smaller number of "orientation bundles" which defined local myofiber orientation.

The various surfaces were then filled with a hexahedral mesh at 0.2-mm resolution. Within the myocardial envelope, a 1-mm layer of myocardium was placed at the endocardial side. This myocardium was given isotropic electrical

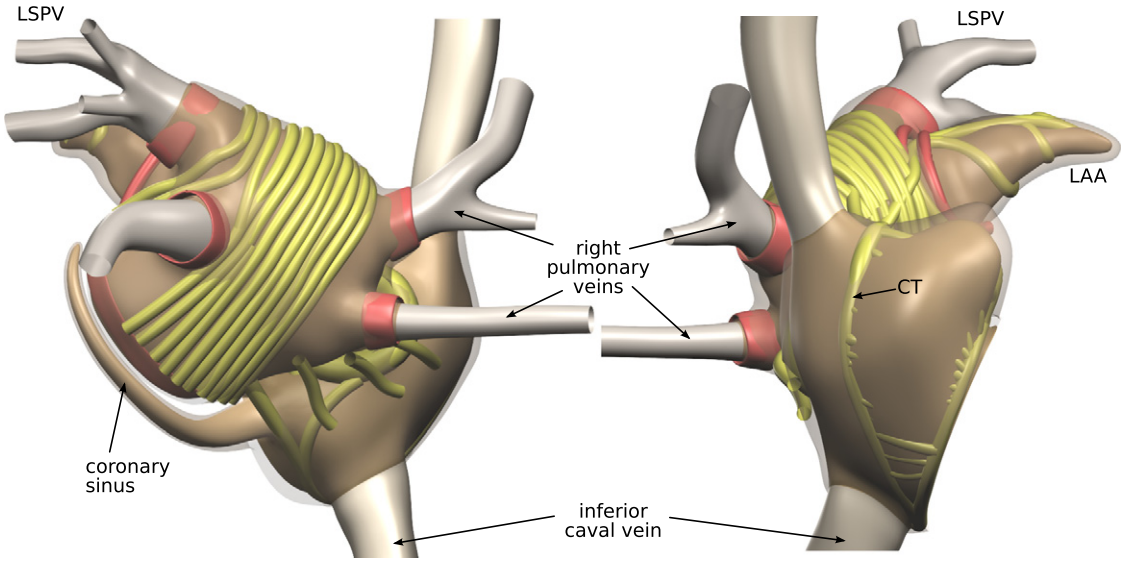

Fig. 1. Anatomic model of the atria used for the simulations. Left panel, posterior view; right panel, right sagittal view. The endocardial surface is rendered in brown; fiber bundles in yellow, "orientation bundles" in red, and the "myocardial envelope" semi-transparently. LSPV, left superior pulmonary vein; LAA, left atrial appendage; CT, crista terminalis.

conductivity, except where it coincided with an orientation bundle (red tubes in Fig. 1); in these places it was made anisotropic with a fiber orientation aligning with the tube's axis. Bundles (yellow tubes in Fig. 1) were filled with anisotropic myocardium with a fiber orientation aligning with the bundle direction.

Simulations of atrial electrical activation were performed using the Propag software (version 4) [18]. Atrial activation was simulated using a monodomain reaction–diffusion equation on a semi-structured mesh with a spatial step size of 0.2 mm. Membrane electrophysiology was represented by the Courtemanche model for the human atrial myocyte [19]. To compute the ECG from the simulated atrial activity we embedded the atrial model in an inhomogeneous torso model including lungs and intracavitary blood masses and solved the bidomain equation at 1-mm resolution [20].

For comparison of measured and simulated P waves, the simulated ECGs were subjected to a low-pass filter with a cut-off frequency of 419 Hz, the same value as the analog filter applied to the measured data. In addition, the simulated P waves were subjected to the same alignment and averaging procedure as the measured data. For this purpose we created a record consisting of only noise and physiological variability by taking the original recording of one subject, subtracting from each of its 366 beats the P wave-aligned average PQRST complex, and superposing the simulated P wave and the subject's averaged QRST complex.

Frequency content

Amplitude spectral densities of measured and simulated 12-lead ECGs were estimated using a discrete Fourier transform. A Hann window was used to minimize frequency aliasing. To estimate the noise spectrum of the measured data the average signal was subtracted from each beat, and the average spectrum of the remaining data in the P-wave interval was computed. To estimate the noise after averaging, the beats were averaged in 5 randomly selected groups. The difference between each group average and the total average was computed and the average spectrum of these difference signals was determined. This spectrum may be expected to overestimate the final noise densities by a factor $\sqrt{5}$ [21,22]. In addition the spectra of the average P wave, QRS complex, and T wave were computed. All spectral densities were averaged over the 12 standard leads.

Statistics

The statistical significance of differences in group mean values of the number of peaks was estimated using Student's *t*-test; $p < 0.05$ was considered significant.

Results

Measurements

The total noise level in the recordings was about 20 μV peak-to-peak. Signal averaging reduced the noise level to less than 2 μV. Fig. 2, panel A, shows the raw data for one lead in one subject. Panel B shows the same signal after low-pass filtering with 150 and 40 Hz cutoff frequencies. With a 150-Hz cutoff, the recommended value [23], there is still noise remaining. With a 40-Hz cutoff, a value often used clinically [24], the signal is smooth, but it cannot be characterized as a simple dome or sine wave. Panel C of Fig. 2 shows the signal after application of our averaging methods, using either alignment on the QRS complex or on the P wave. With P wave-based alignment more small-scale features could be resolved, while either type of alignment resolved the larger features of the P wave. The PQ segment became a single smooth curve, and the 40-ms interval before the P wave became flat, demonstrating that the remaining noise level was less than the thickness of the trace. The remaining features that are visible in the P-wave aligned signal can therefore be assumed to be physiological. Comparison between panels B and C shows that 150-Hz filtering was not enough to remove all interference, and

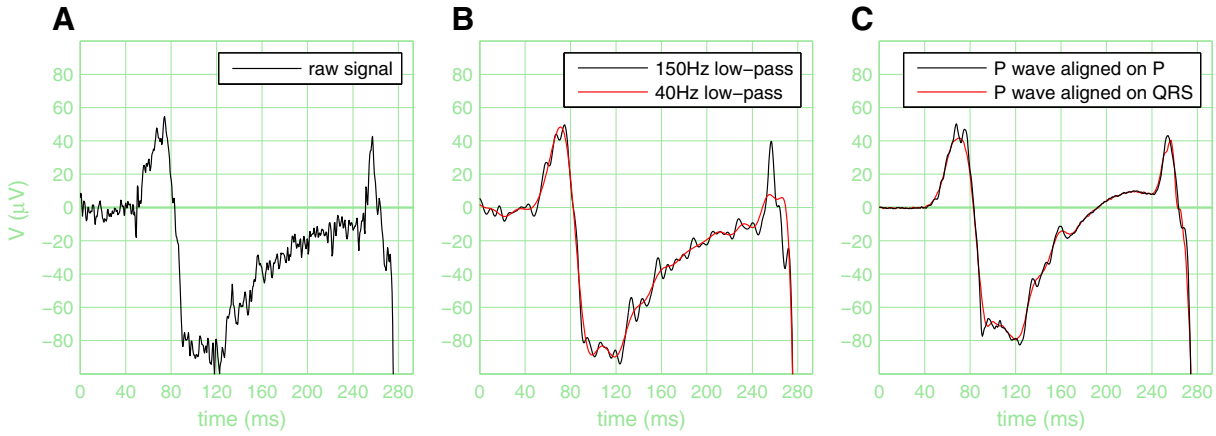

Fig. 2. A: Raw signal for lead V1, after baseline correction. B: The same signal, low-pass filtered at 40 and 150 Hz. C: Signal after averaging 300 beats. Red trace, alignment based on the QRS complex; black trace, alignment based on the P wave. In all panels, only the P wave, PQ interval, and the onset of the QRS complex (clipped) are shown. Horizontal grid lines are 20 μV apart (i.e. 5× normal amplification); vertical grid lines are 40 ms apart (standard). The display starts at the baseline point.

40-Hz filtering deleted physiological signal features. Both types of filtering did not allow the finest details of the P wave to be seen.

An averaged 12-lead ECG of one of the subjects is shown in Fig. 3. Due to the extremely low resulting noise level the P-wave shape and PQ interval are clearly defined. The QRS complexes are slightly smoothed due to the alignment on the P wave and the variability (approximately ±5 ms) in PQ interval.

Average P-wave duration was 104 ms (range 90–129) in the young group and 108 ms (range 87–130) in the senior group.

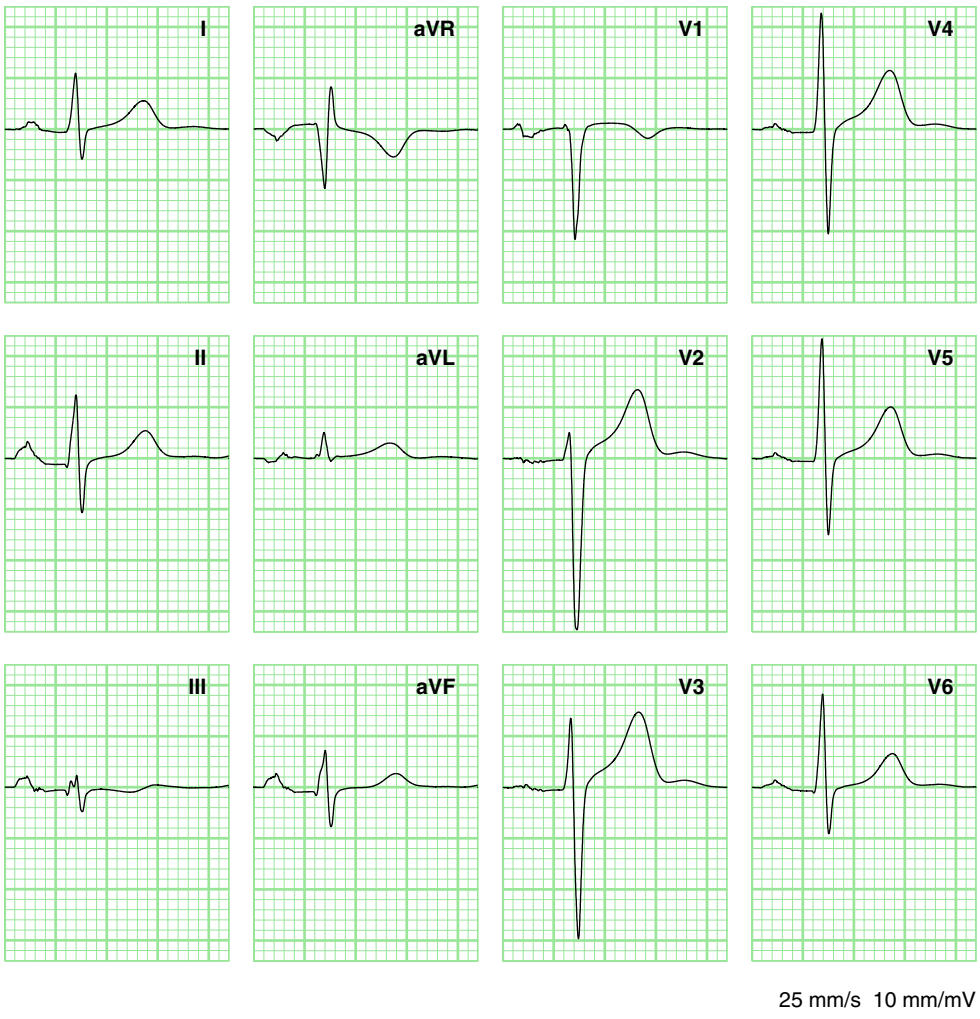

Fig. 3. 12-lead ECG of subject Y2, averaged over 300 beats using alignment on the P wave.

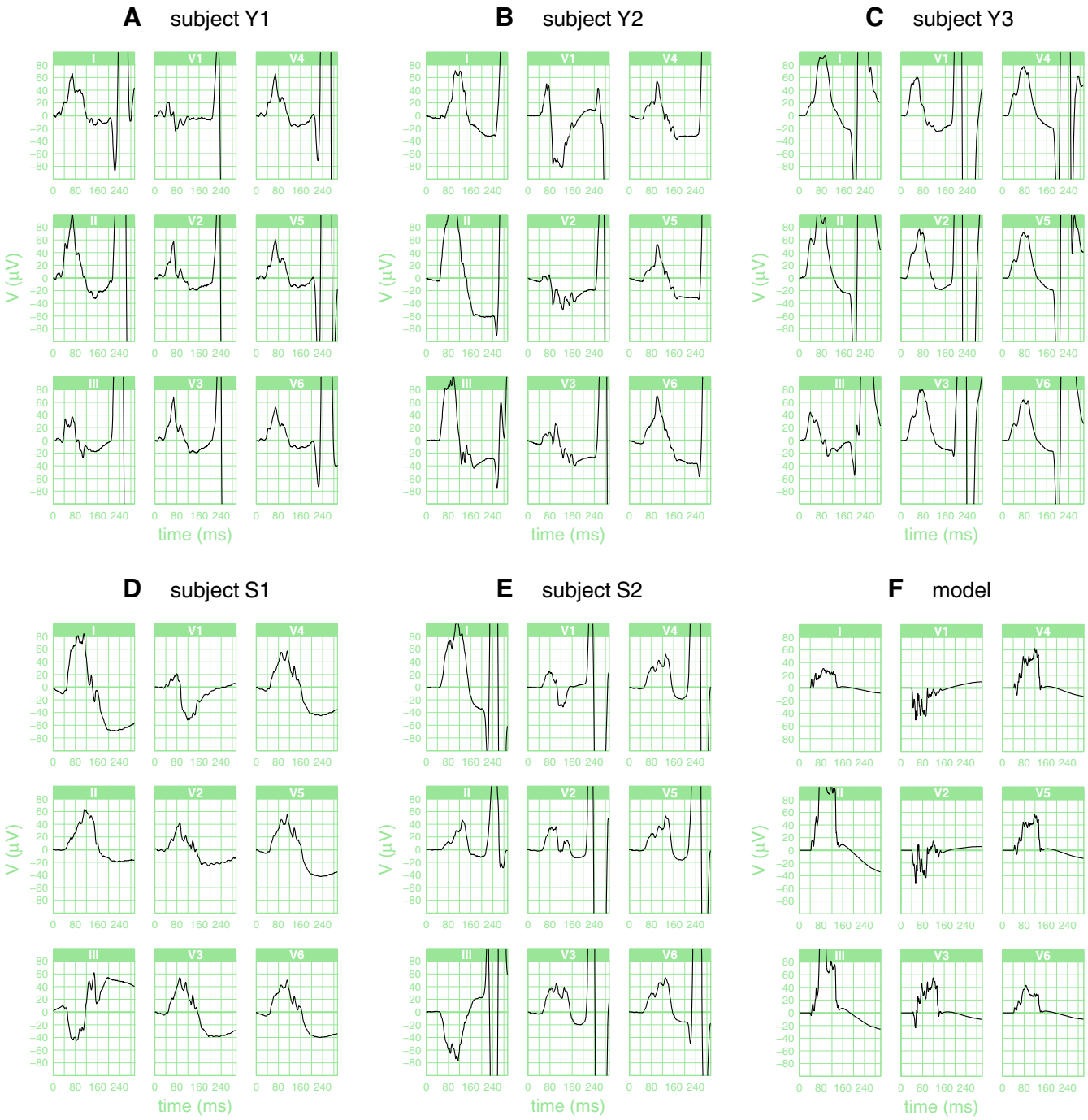

Fig. 4. Selected ECG leads of 5 subjects and the computer model, showing only the P wave, PQ interval, and the onset of the QRS complex (clipped). Signals were averaged over 300 beats using alignment on the P wave. Horizontal grid lines are 20 μV apart (i.e. 5× normal amplification); vertical grid lines are 40 ms apart. The display starts at the baseline point and the zero level coincides with a thicker grid line.

Fig. 4 (panels A–E) shows only the P wave and the PQ interval, at a much larger magnification, for five subjects. Tables 1 and 2 report the number of peaks. To determine the minimum number of invariable peaks that could be demonstrated in each lead, the threshold for the definition of a peak was determined by the variability in that lead in each subject. The results are reported in Table 1. The number of peaks differed between leads and between subjects; the average over all leads and all subjects was 4.1.

A second analysis was performed to compare the number of peaks between leads and between subjects. For this purpose a fixed threshold of 10 μV was used. The results are reported in Table 2, and demonstrate once more large differences between leads and between subjects. No statistically significant differences between the two groups were found.

The analysis of temporal positions of peaks suggested three intervals in which peaks occurred more often than in neighboring intervals. We delineated the intervals of high density as 40–45, 60–75, and 85–100 ms after P-wave onset. In contrast, the first 40 ms of the P-wave had relatively few peaks. The density of peaks was evaluated

Table 1
Lower bounds on the number of stable peaks in each lead for each subject. Averages per lead and per subject are also given.

	I	II	III	aVL	aVR	aVF	V1	V2	V3	V4	V5	V6	Average
Subject Y1	1	1	3	1	4	1	4	2	2	2	2	2	2.1
Subject Y2	1	2	5	1	2	2	8	4	8	3	2	3	3.4
Subject Y3	3	5	5	5	1	5	3	1	1	1	3	5	3.2
Subject Y4	1	5	4	3	1	5	4	4	4	4	3	7	3.8
Subject Y5	4	2	5	3	3	3	2	4	5	7	3	5	3.8
Subject Y6	1	3	3	3	5	3	2	3	3	3	3	3	2.9
Subject Y7	4	5	8	4	6	5	3	3	4	4	4	4	4.5
Average Y	**2.9**	**3.4**	**4.7**	**3.1**	**3.7**	**3.9**	**4.3**	**3.9**	**4.3**	**3.9**	**3.1**	**4.6**	**3.8**
Subject S1	6	6	5	6	8	8	7	6	6	6	6	6	6.3
Subject S2	3	5	3	5	3	2	4	3	3	3	5	3	3.5
Subject S3	2	4	5	2	2	5	4	5	7	5	5	5	4.2
Subject S4	3	5	3	3	3	5	5	5	3	3	6	10	4.5
Subject S5	1	2	3	3	1	2	5	8	8	10	8	1	4.3
Subject S6	3	3	1	3	3	1	1	1	4	4	2	2	2.3
Subject S7	4	4	4	4	3	5	6	5	5	2	6	6	4.5
Subject S8	4	3	7	3	6	6	4	6	5	5	4	5	4.8
Subject S9	9	6	8	6	10	8	7	9	7	7	6	7	7.5
Average S	**3.3**	**4.1**	**4.3**	**3.7**	**3.9**	**4.3**	**4.3**	**4.7**	**5.0**	**4.7**	**5.1**	**4.7**	**4.3**
Average	**3.1**	**3.8**	**4.5**	**3.4**	**3.8**	**4.1**	**4.3**	**4.3**	**4.7**	**4.3**	**4.2**	**4.6**	**4.1**

in 7 temporal bins of varying widths, for each subject individually. Mean and standard deviation for the whole group are reported in Fig. 5. Five differences between adjacent bins were found to be statistically significant, establishing the intervals 60–75 ms and 85–100 ms after P-wave onset as having a relatively high density of peaks.

Simulations

Simulated P waves are shown in panel F of Fig. 4. The signals show slightly more complexity than the measured signals, but similar amplitude and variability in shape.

The effect of different filter setting is illustrated in Fig. 6 using low-pass filter frequencies of 419 Hz, 150 Hz, and 40 Hz. A low-pass frequency of 150 Hz can be seen to affect the smaller features of the P wave, for example the appearance of the first notch in lead III. Such a filter does not affect the global shape of the P wave, including the number of peaks. At a low-pass frequency of 40 Hz, however, many details were lost. The notch in lead III disappeared, and in several places two closely separated peaks merged into one.

When the simulated P wave was superposed on the noise record of subject Y2 and subjected to the same alignment and averaging procedure as the measured data, the recovered 12-lead P wave differed from the original by less than 4 μV (0.46 μV root-mean-square). The traces were visually indistinguishable from those in Fig. 4, panel F.

Frequency content

The spectral densities of subject Y2 are shown in Fig. 7. At a frequency of approximately 60 Hz the P-wave

Table 2
Number of peaks in each lead for each subject, determined using a fixed threshold of 10 μV. Averages per lead and per subject are also given.

	I	II	III	aVL	aVR	aVF	V1	V2	V3	V4	V5	V6	Average
Subject Y1	1	1	3	1	3	1	2	2	2	2	2	2	1.8
Subject Y2	1	2	7	1	4	4	4	10	8	3	2	3	4.1
Subject Y3	1	1	2	1	1	2	1	1	1	1	1	1	1.2
Subject Y4	1	3	4	3	1	5	4	4	4	4	3	1	3.1
Subject Y5	4	1	2	1	3	1	2	4	1	1	1	1	1.8
Subject Y6	1	3	3	3	7	3	2	3	3	3	1	1	2.8
Subject Y7	4	6	5	4	5	5	5	5	2	1	2	5	4.1
Average Y	**1.9**	**2.4**	**3.7**	**2.0**	**3.4**	**3.0**	**2.9**	**4.1**	**3.0**	**2.1**	**1.7**	**2.0**	**2.7**
Subject S1	3	1	1	1	1	2	2	1	3	3	1	1	1.7
Subject S2	4	2	3	2	4	2	3	4	4	4	2	2	3.0
Subject S3	3	3	1	3	3	2	2	2	3	3	3	3	2.6
Subject S4	2	2	3	2	2	1	4	3	3	5	5	5	3.1
Subject S5	3	3	3	3	3	2	3	2	3	3	4	4	3.0
Subject S6	1	2	1	3	1	2	3	4	4	2	2	14	3.2
Subject S7	2	3	1	2	3	1	1	1	2	2	2	2	1.8
Subject S8	4	4	4	4	3	3	4	5	5	3	2	2	3.6
Subject S9	2	3	7	1	4	6	2	6	7	5	4	5	4.3
Average S	**2.7**	**2.6**	**2.7**	**2.3**	**2.7**	**2.3**	**2.7**	**3.1**	**3.8**	**3.3**	**2.8**	**4.2**	**2.9**
Average	**2.3**	**2.5**	**3.1**	**2.2**	**3.0**	**2.6**	**2.8**	**3.6**	**3.4**	**2.8**	**2.3**	**3.2**	**2.8**
p	0.23	0.87	0.29	0.58	0.41	0.43	0.77	0.42	0.47	0.06	0.06	0.14	0.65

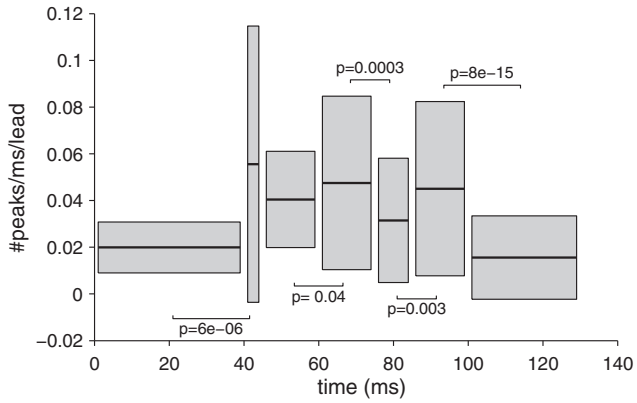

Fig. 5. Mean and standard deviation of the number of peaks per millisecond time and per lead. For each bin, a thick horizontal line indicates the mean, and the gray box ±1 standard deviation. Bin edges were located at 0, 40, 45, 60, 75, 85, 100, and 130 ms after P-wave onset. The p values for the difference between the means of adjacent bins are indicated if they classify as statistically significant ($p < 0.05$).

amplitude density drops below the original noise level. Around 200 Hz it reaches the final noise level, but at that frequency it is already 2 orders of magnitude smaller than at 10 Hz, so that it has little influence on the total signal. The P-wave signal content below 40 Hz was 83%. An additional 14% was contained in the band 40–150 Hz, and 3% in still higher frequencies.

Discussion

We have shown that both measured and simulated P waves in subjects with normal atria have a complex shape. P waves had 4.1 distinct peaks on average, while up to 10 peaks could be identified in some cases. Peaks were relatively rare in the first 40 ms of the P wave, and relatively common in the intervals 60–75 and 85–100 ms after P-wave onset.

Contemporary textbooks show the P wave as a half circle or, in the biphasic case, as a sine wave [1,25]. Incidental reports on nonfiltered averaged P waves have demonstrated complexity similar to our results [9–11], but this knowledge is not reflected in the recent medical literature. Not only textbooks, but also original reports show very smooth P waves [26,27]. Using more recent technology and an approach targeted at precise alignment of P waves, we have confirmed the complex shapes shown in the older reports. In addition, our study is the first to systematically investigate the detailed shape of the P wave in the 12-lead ECG.

The smooth P-wave shapes shown in recent literature may be explained by low-pass filtering and perhaps inaccurate alignment of the P waves in averaging procedures. In patients with variable P-wave shapes, it may be very challenging to obtain good alignment, since the waves should at the same time be divided into clusters representing different physiological signals [28]. Even in our normal subjects, comparison of raw and averaged signals occasionally suggested that details had been smoothed out by averaging. In clinical practice, the small size at which P waves are typically printed, the thickness of the trace, and the aspect ratio which is more suitable for QRST complexes further contribute to an underestimation of P-wave complexity. However, the current generation of ECG systems stores the data digitally and essentially unfiltered, allowing the viewer to select the filter characteristics. Some systems also allow the user to zoom in or change the amplification. These advances will allow clinicians to see more details of the P wave.

Noise and interference generated at the electrode-skin interface, in the wiring, and in the amplifier are inevitable in ECG recordings. Low-pass filtering is a common method to

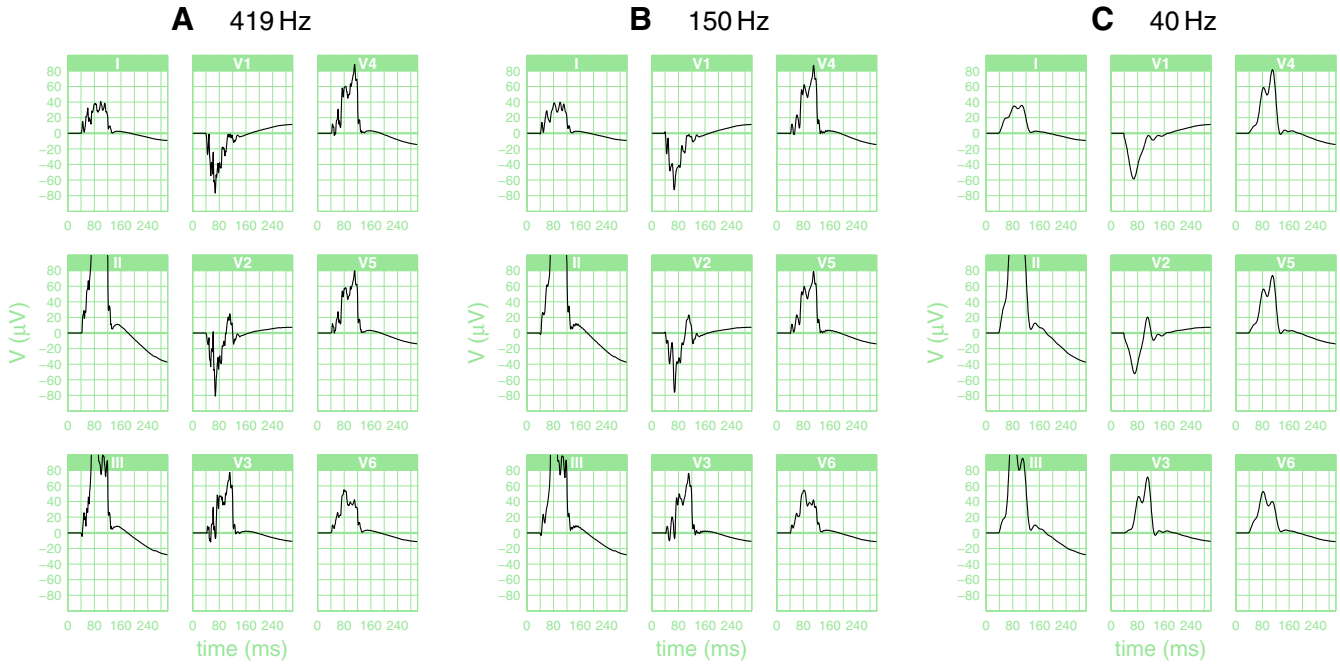

Fig. 6. Simulated P waves low-pass filtered at (A) 419 Hz (same as measured signals); (B) 150 Hz (guidelines); and (C) 40 Hz.

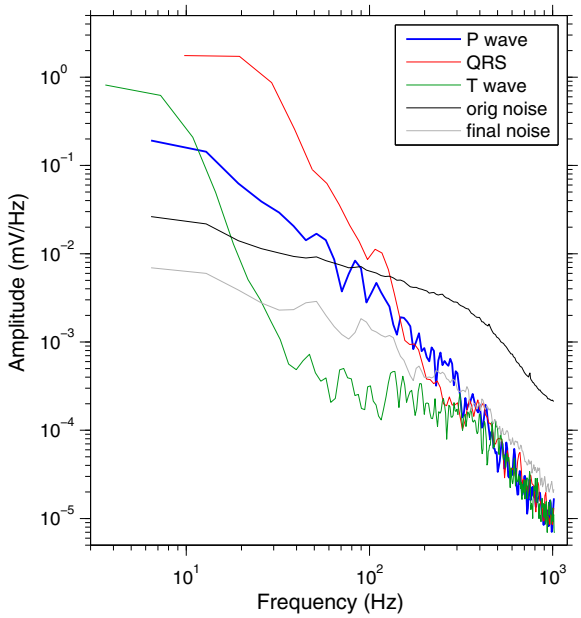

Fig. 7. Amplitude spectral density of the original and averaged record of subject Y2. The lowest measured frequency depended on the length of the associated interval. In blue, red, and green, the spectra of the averaged P wave, QRS complex, and T wave are shown. The spectrum of the original recording noise (black) was averaged over all beats and is therefore smoother than the other spectra. The final noise spectrum (gray) was computed from 5 group averages and therefore overestimates the noise after averaging all beats.

reduce this noise at least for high frequencies, but it also removes the high-frequency part of the signal. Selection of the cut-off frequency is therefore important. Guidelines recommend a frequency of at least 100 Hz [29] and preferably 150 Hz [23]. However, according to one report 53% of routine ECGs were observed with a low-pass filter frequency of 40 Hz, and another 17% at filter frequencies ranging from 30 to 35 Hz [24]. As shown in Figs. 2 and 6, the true shape of the P wave cannot be observed using such filter settings. Our spectral analysis showed that 17% of the P-wave signal is contained in frequencies above 40 Hz, and 3% above 150 Hz. Yet, filtering at 150 Hz would not suffice to recover 97% of the true P-wave shape, because there is significant noise content below that frequency (Figs. 2 and 7). In contrast to filtering, averaging can remove noise in the same frequency band as the signal without removing the signal itself.

The methods that we used to obtain detailed P-wave shapes included several nonstandard components: 1) recording techniques with very low interference; 2) a large number of channels allowing us to suppress noise in the alignment signal by spatial averaging; 3) long recordings (5 or 10 min) to allow averaging; and 4) alignment by maximizing correlation between P waves. Averaging with P-wave alignment was previously used by Havmoller at al. [26] and by subsequent studies from the same group [30,28]. Nevertheless, the P waves they have shown were much smoother than ours. This may be due to their use of a 50 Hz mains filter, higher initial noise levels, or P-wave variability in their patient group.

Although the number of peaks was the same in simulated as in measured P waves, the simulated waves had a more complex shape related to deeper troughs between the peaks. This may be due to the crude representation of anatomical features in our model. In the real atria, transitions from thick bundles to thinner myocardium are probably much smoother than in the model. An alternative explanation is that our averaging methods still result in some smoothing of signals, for example due to slight variations in P-wave shape, and that in fact the physiological P wave is even more complex than we could measure. Using a simulated P wave superposed on a realistic noise record of 366 beats we verified that our alignment and averaging method did not perceptibly distort the shape of a simulated P wave.

Another striking difference between the model and the measured results is the presence of large PQ offsets in the measured leads, which were also highly variable between subjects. We assume that these offsets are part of the Ta waves, the remainder of which is masked by the QRS complex. In the model, Ta waves occurred later and had smaller amplitude. Nonzero potentials in the PQ interval can also be caused by propagation in the AV node and bundle of His. However, we think that this cannot fully explain the observed PQ offsets. His-bundle potentials have an ascending slope over a duration of about 40 ms and an amplitude of approximately 10 μV [10]. In contrast, we observed PQ segments with amplitudes that were several times larger and nearly flat. Moreover, the observed offsets were negative in lead II, where a positive His-bundle potential would be expected.

Limitations

The method described here required a large number of electrodes and some manual intervention. Clinical applicability could be improved by further automation and tests with a smaller number of electrodes. Our method to determine P-wave duration was somewhat subjective.

Financial support

This study was supported by the 7th Framework Program of the European Union through a Marie Curie International Reintegration grant (number 256493) to M.P. and through the collaborative project EUTRAF (number 261057).

A.C.L. was supported by the Dutch Technology Foundation STW under grant number 10959.

Simulations were performed on an SGI Altix 4700 supercomputer at Université de Montréal, operated by Calcul Québec and Compute Canada, and financed by the Canada Foundation for Innovation (CFI), NanoQuébec, RMGA, and the Fonds de recherche du Québec - Nature et technologies (FRQ-NT).

References

[1] Wagner GS. Marriott's Practical Electrocardiography. 9th ed. Baltimore, Maryland, USA: Williams & Wilkins; 1994.

[2] Kabutoya T, Ishikawa S, Ishikawa J, Hoshide S, Kario K, the JMS Cohort Study Investigators Group. P-wave morphologic characteristics predict cardiovascular events in a community-dwelling population. Ann Noninvasive Electrocardiol 2012;17:252–9.

[3] Bayés de Luna A, Platonov PG, Cosio FG, et al. Interatrial blocks. A separate entity from left atrial enlargement: A consensus report. J Electrocardiol 2012;45:445–51.

[4] Agarwal YK, Aronow WS, Levy JA, Spodick DH. Association of interatrial block with development of atrial fibrillation. Am J Cardiol 2003;91:882.
[5] Holmqvist F, Platonov PG, Carlson J, Zareba W, Moss AJ. Altered interatrial conduction detected in MADIT II patients bound to develop atrial fibrillation. Ann Noninvasive Electrocardiol 2009;14:268–75.
[6] Goyal S, Spodick D. Electromechanical dysfunction of the left atrium associated with interatrial block. Am Heart J 2001;142:823–7.
[7] Ogawa M, Kumagai K, Vakulenko M, Yasuda T, Siegerman C, Garfinkel A, et al. Reduction of P-wave duration and successful pulmonary vein isolation in patients with atrial fibrillation. J Cardiovasc Electrophysiol 2007;18:931–8.
[8] Krueger MW, Rhode K, Weber FM, Keller DUJ, Caulfield D, Seemann G, et al. Patient-specific volumetric atrial models with electrophysiological components: A comparison of simulations and measurements. Biomed Tech 2010;55(Suppl 1):54–7.
[9] Jesus S, Rix H. High resolution ECG analysis by an improved signal averaging method and comparison with a beat-to-beat approach. J Biomed Eng 1988;10:25–32.
[10] Peper A, Jonges R, Losekoot TG, Grimbergen CA. Recording of surface His-Purkinje potentials. Med Biol Eng Comput 1985;23(4):365–76.
[11] Langley P, Murray A. Analysis of the atrial repolarisation phase of the electrocardiogram in health and in atrial fibrillation. Comput Cardiol 2007;34:785–8.
[12] Lankveld TAR, Zeemering S, Crijns HJGM, Schotten U. The ECG as a tool to determine atrial fibrillation complexity. Heart 2014;100:1077–84.
[13] Schram MT, Sep SJ, van der Kallen CJ, Dagnelie PC, Koster A, Schaper N, et al. The Maastricht Study: An extensive phenotyping study on determinants of type 2 diabetes, its complications and its comorbidities. Eur J Epidemiol 2014;29:439–51.
[14] Pan J, Tompkins WJ. A real-time QRS detection algorithm. IEEE Trans Biomed Eng 1985;32(3):230–6.
[15] Ho SY, Anderson RH, Sánchez-Quintana D. Atrial structure and fibres: Morphologic bases of atrial conduction. Cardiovasc Res 2002;54:325–36.
[16] Ho SY, Sánchez-Quintana D. The importance of atrial structure and fibers. Clin Anat 2009;22:52–63.
[17] Anderson RH, Becker AE. Cardiac anatomy: An integrated text and colour atlas. London: Gower Medical Publishing; 1980.
[18] Potse M, Dubé B, Richer J, Vinet A, Gulrajani RM. A comparison of monodomain and bidomain reaction–diffusion models for action potential propagation in the human heart. IEEE Trans Biomed Eng 2006;53(12):2425–35.
[19] Courtemanche M, Ramirez R, Nattel S. Ionic mechanisms underlying human atrial action potential properties: Insights from a mathematical model. Am J Physiol Heart Circ Physiol 1998;275:H301–21.
[20] Potse M, Dubé B, Vinet A. Cardiac anisotropy in boundary-element models for the electrocardiogram. Med Biol Eng Comput 2009;47:719–29.
[21] Hoke M, Ross B, Wickesberg R, Lütkenhöner B. Weighted averaging – theory and application to electric response audiometry. Electroencephalogr Clin Neurophysiol 1984;57:484–9.
[22] Sörnmo L, Johansson ET, Simson MB. The signal-averaged electrocardiogram. In: P.W. Macfarlane, A. van Oosterom, M. Janse, P. Kligfield, J. Camm and O. Pahlm, (Eds), Comprehensive electrocardiology, vol. 4. Springer; 2011. p. 1793–821.
[23] Kligfield P, Gettes LS, Bailey JJ, et al. Recommendations for the standardization and interpretation of the electrocardiogram; Part I: The electrocardiogram and its technology; a scientific statement from the American Heart Association Electrocardiography and Arrhythmias Committee, Council on Clinical Cardiology; the American College of Cardiology Foundation; and the Heart Rhythm Society. Heart Rhythm 2007;4:394–412.
[24] Kligfield P, Olgin PM. Prevalence and clinical implications of improper filter settings in routine electrocardiography. Am J Cardiol 2007;99:711–3.
[25] Macfarlane PW, Veitch Lawrie TD. The Normal Electrocardiogram and Vectorcardiogram. In: Macfarlane PW, van Oosterom A, Janse M, Kligfield P, Camm J, Pahlm O, editors. Comprehensive electrocardiology, vol. 2. Springer; 2012.
[26] Havmoller R, Carlson J, Holmqvist F, Herreros A, Meurling CJ, Olsson B, et al. Age-related changes in P wave morphology in healthy subjects. BMC Cardiovasc Disord 2007;7:22.
[27] Platonov PG. P-wave morphology: Underlying mechanisms and clinical implications. Ann Noninvasive Electrocardiol 2012;17:161–9.
[28] Huo Y, Holmqvist F, Carlson J, Gaspar T, Hindricks G, Piorkowski C, et al. Variability of P-wave morphology predicts the outcome of circumferential pulmonary vein isolation in patients with recurrent atrial fibrillation. J Electrocardiol 2015;48:218–25.
[29] Pipberger HV, Arzbaecher RC, Berson AS, Briller SA, Brody DA, Flowers NC, et al. Recommendations for standardization of leads and specifications for instruments in electrocardiography and vectorcardiography. Circulation 1975;52:11–31 [Suppl.].
[30] Holmqvist F, Husser D, Tapanainen JM, Carlson J, Jurkko R, Xia Y, et al. Interatrial conduction can be accurately determined using standard 12-lead electrocardiography: Validation of P-wave morphology using electroanatomic mapping in man. Heart Rhythm 2008;5:413–8.